Electronic Supplementary Material (ESI) for Inorganic Chemistry Frontiers.
This journal is © the Partner Organisations 2021

Supporting Information

Optimization of metal-organic framework derived transition metal hydroxide hierarchical arrays for high performance hybrid supercapacitors and alkaline Zn-ion batteries

You Wang,[†] Teng Wang,[†*] Jiaqi Lei, and Kai-jie Chen*

Key Laboratory of Special Functional and Smart Polymer Materials of Ministry of Industry and Information Technology, Xi'an Key Laboratory of Functional Organic Porous Materials, Department of Chemistry, School of Chemistry and Chemical Engineering, Northwestern Polytechnical University, Xi' an, Shaanxi 710072, PR China.

Email: wangt42@nwpu.edu.cn; ckjiscon@nwpu.edu.cn.

Experimental section

Chemicals: All the chemicals of analytical grade from Aladdin (Shanghai Aladdin Bio-Chem Technology Co., LTD) were used as received without further purification. Deionized water with a resistivity of 18.25 MΩ cm was used. Carbon fiber clothes were provided by ElectroChem Inc (USA). Zinc plates, positive and negative electric casings, gaskets, and shrapnel were purchased from Corud, and the glass microfiber filters came from Whatman.

Modification of carbon fiber clothes (CFCs)

The CFCs were functionalized by immersing into HNO_3/H_2SO_4 (3:1) solution for 2 h to obtain a highly hydrophilic surface before being cleaned by acetone and ethanol under sonication for 10 min in sequence.

Preparation of precursor $Co(OH)_2$ nanowire arrays

The $Co(OH)_2$ nanowire arrays were synthesized by a facile hydrothermal method. $Co(NO_3)_2 \cdot 6H_2O$ (0.03 M,0.1746 g) were completely dissolved in 10 mL of ultrapure water and kept stirring for 10 minutes. NH_4F (0.09 M, 0.0667 g) and $CO(NH_2)_2$ (0.15 M, 0.1802 g) were completely dissolved in 10 mL of ultrapure water under ultrasonication for 5 minutes, which were then poured into the Co^{2+} contained solution and kept stirring for 30 min to form a transparent pink colored solution. The resulting reaction solution was then transferred to a 20 mL Teflon-lined stainless steel autoclave and a piece of clean carbon fiber cloth (CFC, 1 x 4 cm^2) was immersed into the solution. The autoclave was put in an electric oven for hydrothermal reaction under 120 ºC for 8 h. After the reaction, the product was rinsed with ultrapure water three times and then dried in a vacuum oven at 60 ºC for another 8 h.

Preparation of $Co(OH)_2$@ZIF-67 hybrid arrays

2-methylimidazole (2-MIM, 0.6 M, 1.2315 g) was dissolved into 25 mL ultrapure water. The $Co(OH)_2$ nanowire arrays were immersed into the 2-MIM solution for 24 h at room temperature to form $Co(OH)_2$@ZIF-67 hybrid. Then the sample was rinsed with ultrapure water three times and then dried in a vacuum oven at 60 ºC for 8 h.

Preparation of A-$Co(OH)_2$@ZIF-67 hybrid arrays

The obtained $Co(OH)_2$@ZIF-67 was placed in a tube furnace and then heated under 350 ºC for 30 min in a nitrogen atmosphere with a ramping rate of 5 ºC/min. The annealed sample was named as A-$Co(OH)_2$@ZIF-67.

Preparation of A-$Co(OH)_2$@NiCo-LDH arrays

The annealed sample was transferred into a glass bottle that contained $Ni(NO_3)_2$•$6H_2O$ (0.1 M, 0.4225 g) and 25.0 mL ethanol. The reaction was carried out at room temperature for 24 h. Then the product was collected and rinsed with ultrapure water three times and put into a vacuum oven at 60 ºC for 8 h. The mass loading of A-$Co(OH)_2$@NiCo-LDH is 1.0 - 2.0 mg cm^{-2}. Note that the mass loading of the active materials can be increased by growing the materials on functionalized CFCs with higher surface area.

Material Characterization

The microstructures and compositions of all samples were analyzed by field emission scanning electron microscope (SEM, Verios G4, FEI), transmission electron microscopy (TEM, FEI Talos F200X), X-ray photoelectron spectroscopy (XPS, Kratos AXIS Ultra DLD), Raman spectroscopy (Raman, WITec, Germany), N_2 gas sorption

test (Micromeritics 3Flex), and X-ray diffraction analysis (XRD, Rigaku Mini Flex 600 with Cu Kα radiation).

Electrochemical Measurements

All electrochemical measurements were carried out with an electrochemical workstation (VSP, BioLogic) at room temperature (25 ºC). The electrochemical impedance spectrum (EIS) of the material was obtained in the frequency range from 200 kHz to 10 mHz with an AC potential amplitude of 5 mV at zero DC voltage. The cycling stability of the as-synthesized materials was tested using a program-control automatic system (LANHE-CT3001A). The accuracy of the electronic balance is d = 0.01 mg (METTLER TOLEDO-ME55)

Three-electrode test system

The as-synthesized materials were used as the working electrode. A square platinum foil (1x 2 cm^2) was employed as the counter electrode and Hg/HgO electrode was applied as the reference electrode. 2.0 M KOH aqueous solution was utilized as the electrolyte.

To acquire the specific capacity (Q, mAh g^{-1}) and specific capacitance (C_s, F g^{-1}) of the electrode, Galvanostatic charge/discharge (GCD) tests were performed and the corresponding data were obtained based on the following formula (1-2)[1]:

$$Q = \frac{1}{3.6} \times \frac{I\int_{t_i}^{t_f} V dt}{mU_{mean}} = \frac{1}{3.6} \times \frac{I\int_{t_i}^{t_f} V dt}{m \times \frac{U}{2}} = \frac{1}{1.8} \times \frac{I\int_{t_i}^{t_f} V dt}{mU} \quad (1)$$

$$C_s = \frac{I\int_{t_i}^{t_f} V dt}{m\int_{v_i}^{v_f} V dV} = \frac{I\int_{t_i}^{t_f} V dt}{\frac{1}{2}V^2\Big|_{t_i}^{t_f}} \quad (2)$$

Where I (A) is the current response, t_i and t_f are the initial and final values of discharge

time t (s). m (g) is the mass loading and V (V) is the operating potential. U_{mean} (V) is the mean value of V, and U (V) is the potential window.

The dynamic electric energy storage mechanism of A-Co(OH)$_2$@NiCo-LDH arrays was analyzed by running cyclic voltammetry (CV) experiments. The relationship of current response *vs* scan rates in CV curves can be presented by formula (3): [2, 3]

$$i_{(v)} = av^b \Rightarrow \log i = b \log v + \log a \quad (3)$$

Where i is current, v is the scan rate, and both a and b are adjustable parameters. b = 1 indicates the energy storage process is dominated by pseudocapacitive behavior while b = 0.5 means the mechanism is mainly based on a battery-like redox reaction behavior.

The capacitive contribution of the electrode materials at different CV scans was analyzed based on the peak current at different anodic scanning rates for the active materials according to the reported method.[4, 5] Specifically, k_1 and k_2 can be obtained by plotting $v^{1/2}$ versus $i/v^{1/2}$ according to equation (4).[6]

$$i(V) = k_1 v + k_2 v^{\frac{1}{2}} \Rightarrow \frac{i(V)}{v^{\frac{1}{2}}} = k_1 v^{\frac{1}{2}} + k_2 \quad (4)$$

where i (V) is the anodic peak current and v is the corresponding scan rate. k_1v/i is the capacitive contribution ratio, and $k_2v^{1/2}/i$ is the surface diffusion controlled redox reaction contribution ratio.

Assembly of hybrid supercapacitor and alkaline zinc ion batteries

Fabrication of hybrid supercapacitor (HSC)

The HSC device was assembled by using A-Co(OH)$_2$@CoNi-LDH electrode as cathode, activated carbon (AC) electrode as anode, and 2 M KOH as the electrolyte.

The mass ratio of the active materials of cathode and anode was balanced using the following equation (5):[7]

$$\frac{m_+}{m_-} = \frac{C_- \times \Delta V_-}{Q_+} \quad (5)$$

Where Q_+ (mAh g^{-1}) and C_- (F g^{-1}) represent the gravimetric specific capacity of the cathode electrode and specific capacitance of the anode electrode, respectively. ΔV_- is the potential window of anode. m_+ (g) and m_- (g) are the mass of the cathode and anode electrodes respectively. Practically, in the best performed HSC, the A-$Co(OH)_2$@CoNi-LDH had a mass loading of 1.35 mg and the activated carbon (AC) electrode had a mass of 2.91 mg.

The energy density (E, Wh kg^{-1}), power density (P, W kg^{-1}), and Coulombic efficiency (η_E) were calculated based on equations (6-8) [8, 9]:

$$E = \frac{I\int_{t_i}^{t_f} V_s dt}{3.6m} \quad (6)$$

$$P = \frac{3600 \times E}{\Delta t} \quad (7)$$

$$\eta_E = \frac{E_D}{E_C} \quad (8)$$

Where m (g) is the total mass of positive and negative electrode materials. V_s (V) is the operating voltage. t_i and t_f are the initial and final values of discharge time t (s). E_C and E_D are the charge and discharge energy density (Wh kg^{-1}).

Assembly of alkaline zinc ion batteries (AZIBs)

The AZIB was prepared by assembling the A-$Co(OH)_2$@CoNi-LDH cathode with a mass of 1.07 mg (1×1 cm^2) and Zn anode (1×1 cm^2) with an alkaline electrolyte (6

M KOH and 0.2 M $Zn(CH_3COO)_2$, 150 μL).

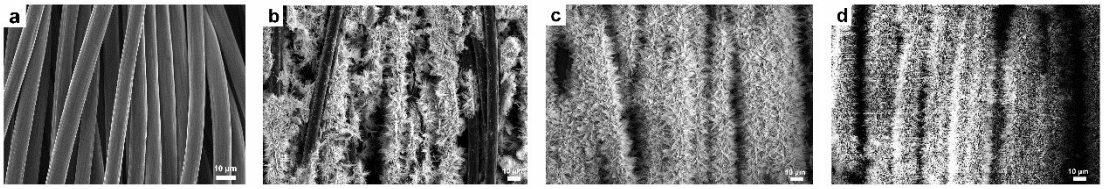

Fig. S1. (a) SEM images of pure CFC substrate, $Co(OH)_2$ nanowire arrays grown on (b) un-treated and (c) modified CFCs; (d) SEM images of $Co(OH)_2$ nanowire arrays grown on modified CFCs after ultrasound treatement.

In order to verify the effect of CFC surface modification, the SEM images of $Co(OH)_2$ nanowire arrays on unmodified and modified CFC were obtained (Figure S1b and Figure S1c). It is clear that the nanowires were densely grafted on acid-treated hydrophilic CFC while the $Co(OH)_2$ only randomly distributed on the un-treated CFC. This confirms that the hydrophilic surface modification of the CFC contributes to the adsorption of the Co^{2+}, nucleation, and directional growth of the $Co(OH)_2$ nanowires. To test the binding force of nanowires with CFC, we ultrasonicated the sample for 5 minutes in deionized water, which still remained very well array structure (shown in Figure S1d), demonstrating the intimate contact between the nanowires and the CFC substrate.

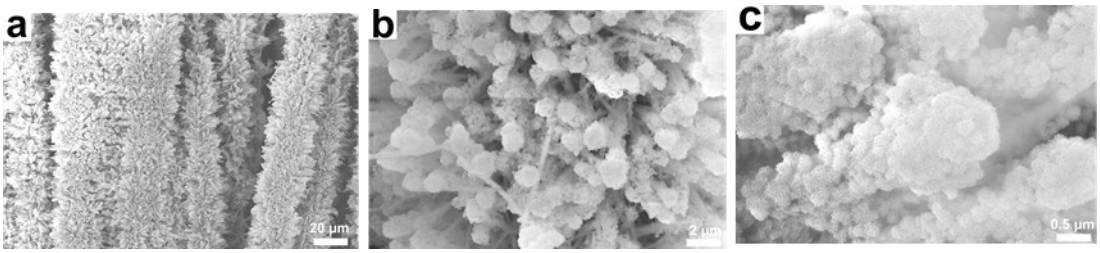

Fig. S2. (a-c) SEM images of $Co(OH)_2$@NiCo-LDH.

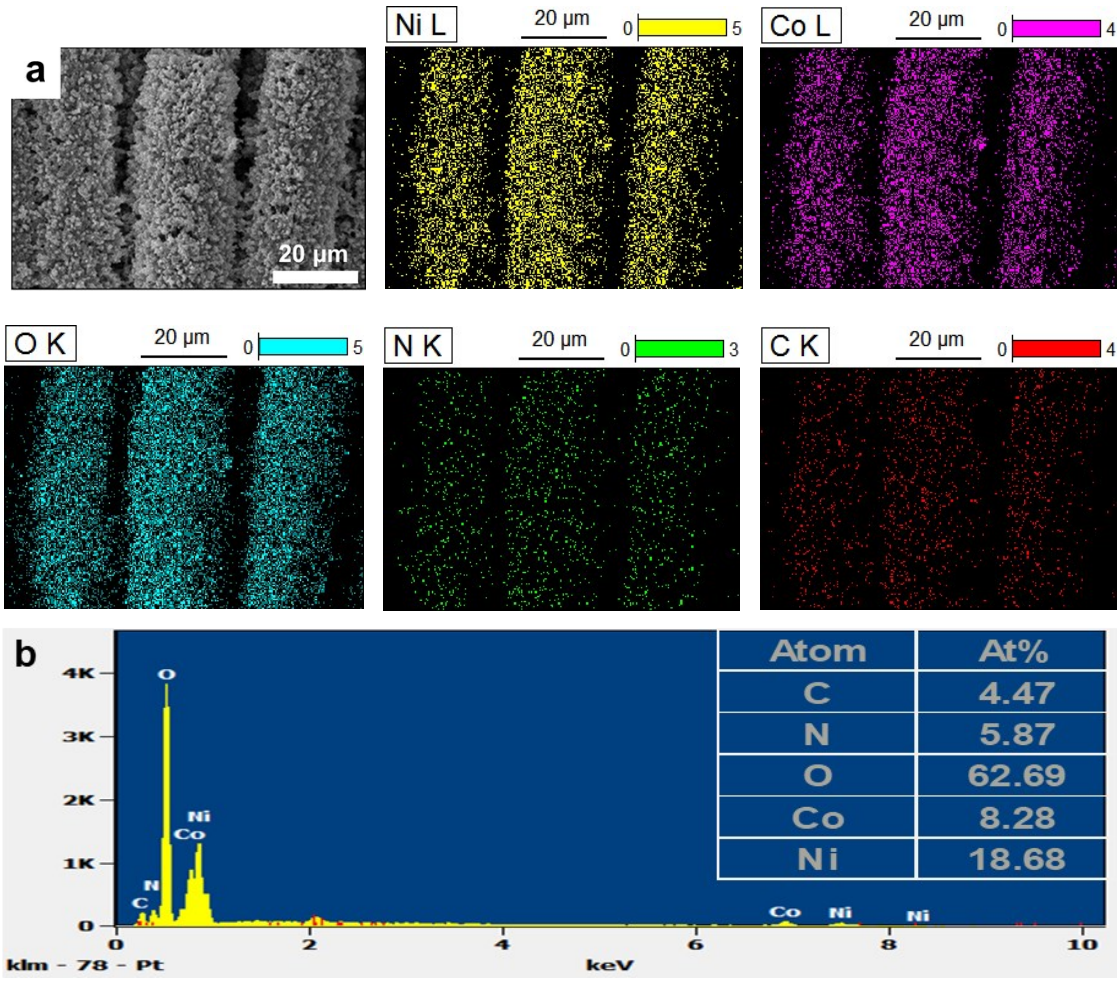

Fig. S3. (a) SEM and EDS elemental mapping images of A-$Co(OH)_2$@NiCo-LDH; (b) EDS spectrum of A-$Co(OH)_2$@NiCo-LDH.

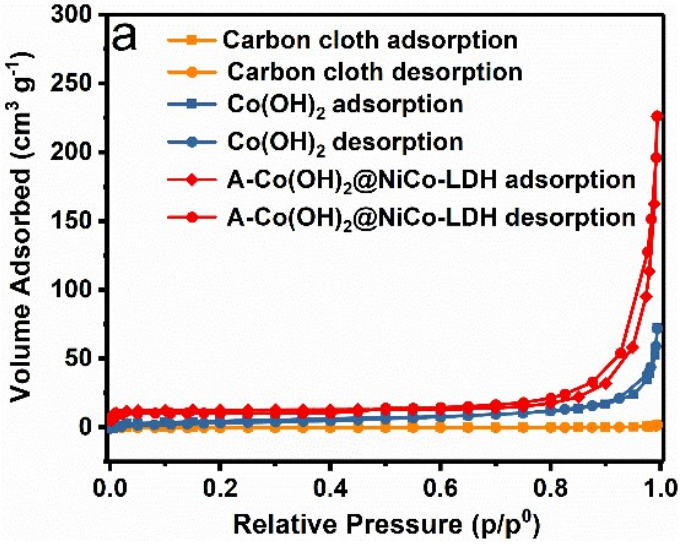

Fig. S4 N_2 adsorption-desorption isotherm of bare CFCs (a), $Co(OH)_2$ (b), and A-$Co(OH)_2$@NiCo-LDH (c) at 77 K and pressure of 0 – 1.0 bar, respectively.

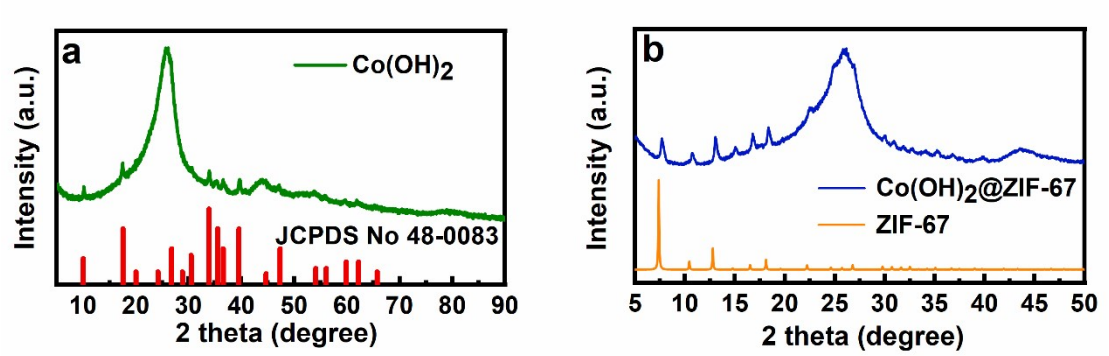

Fig. S5. (a) XRD patterns of $Co(OH)_2$ and the corresponding standard sample; (b) XRD patterns of $Co(OH)_2$@ZIF-67 and standard ZIF-67.

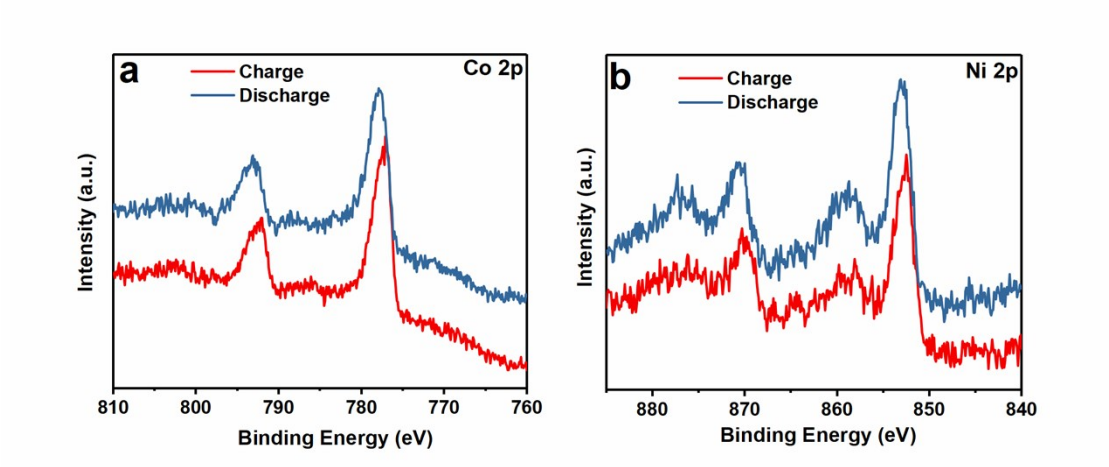

Fig. S6. High-resolution XPS spectra of Co 2p (a) and Ni 2p (b) in A-$Co(OH)_2$@NiCo-LDH at charge (+0.55 V *vs* Hg/HgO) and discharge (+0 V *vs* Hg/HgO) states.

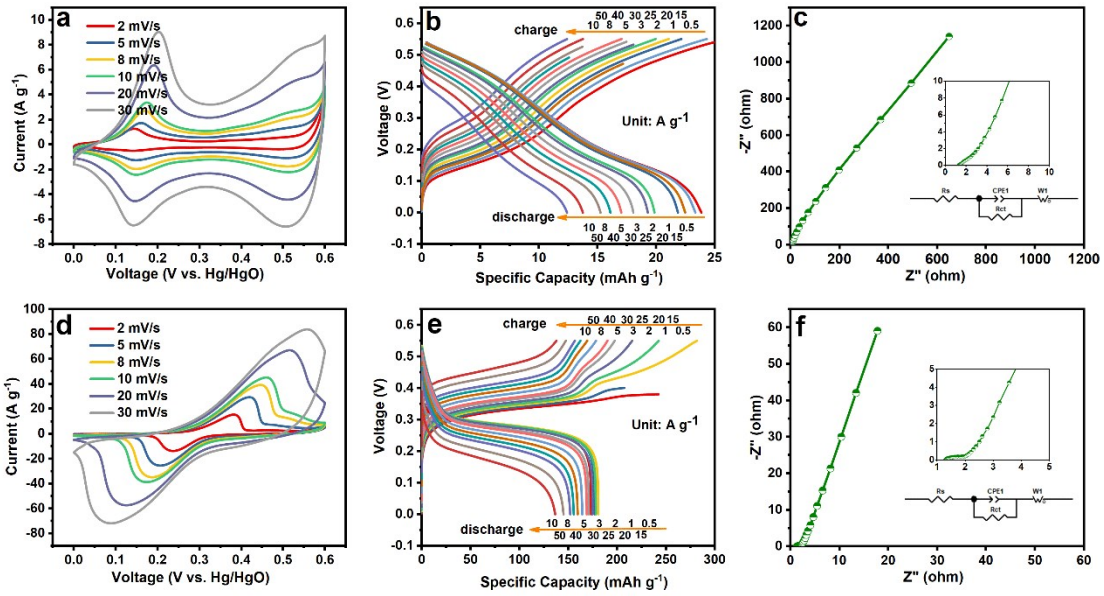

Fig. S7. CV with different scanning rates, GCD curves with different current densities, and EIS spectrum of $Co(OH)_2$ nanowire arrays (a-c) and $Co(OH)_2$@NiCo-LDH composite arrays (d-f), respectively.

Table S1. The fitted series resistance (R_s) and charge transfer resistance (R_{ct}) values of $Co(OH)_2$-NWA, $Co(OH)_2$@NiCo-LDH, and A-$Co(OH)_2$@NiCo-LDH.

Resistance	$Co(OH)_2$-NWA	$Co(OH)_2$@NiCo-LDH	A-$Co(OH)_2$@NiCo-LDH
R_s (Ω)	1.30	1.22	1.50
R_{ct} (Ω)	0.35	1.13	0.34

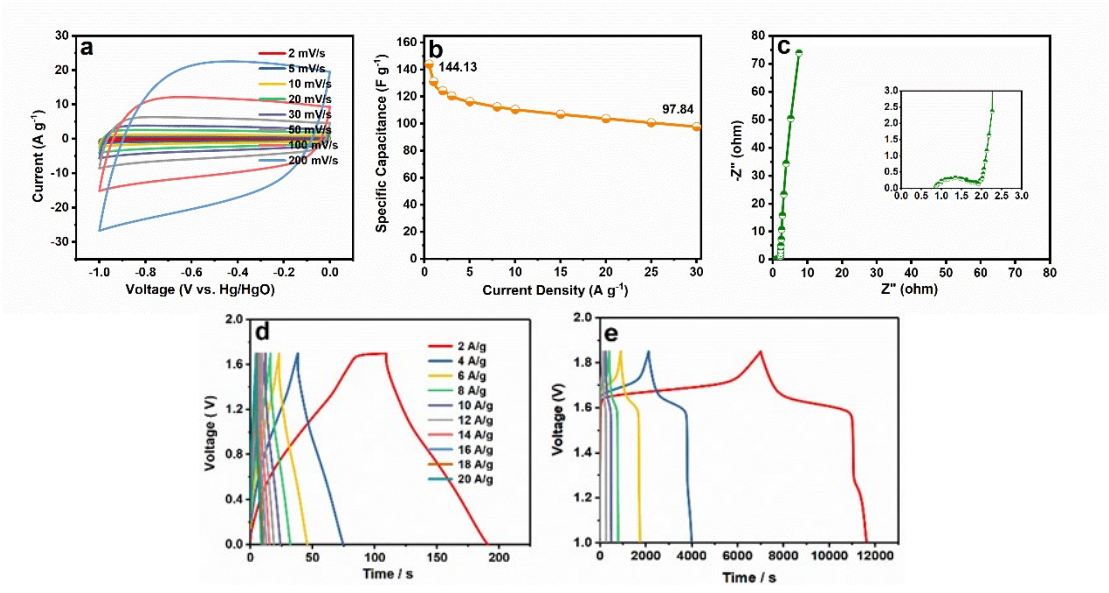

Fig. S8. (a-c) Capacitive performance of activated carbon: (a) CV with different scanning rate; (b) specific capacitance with different current density; (c) EIS spectrum of the activated carbon electrode. The inset is the enlarged EIS spectrum. (d) GCD

curves of HSC; (e) GCD curves of AZIB.

Table S2. The supercapacitive performance comparison of the state-of-the-art supercapacitors based on transition metal compounds

Supercapacitors	Voltage window (V)	Specific capacitance	Energy density (E, Wh kg^{-1})	Power density (P, kW kg^{-1})	Capacitance retention rate	Ref.
NiCo-LDH/Co_9S_8//AC	1.6	106 F g^{-1} at 1.0 A g^{-1}	38 at the P of 0.8	8 at the E of 31.1	93.1% after 5000 cycles at 1 A g^{-1}	10
NCLDH@CNTs//AC	1.5	-	32.5 at the P of 0.15	6.584 at the E of 15	78.7% after 8000 cycles at 1 A g^{-1}	11
NiCo-LDH@PANI@CC//AC	1.6	79.3 F g^{-1} at 0.5 A g^{-1}	26.5 at the P of 0.73	6.2 at the E of 8.4	78% after 5000 cycles at 5 A g^{-1}	12
CoNi-MOF//AC	1.5	-	28.5 at the P of 1.5	24 at the E of 13.3	96 % after 5000 cycles at 16 A g^{-1}	13
NiCo-LDH/NCF//AC	1.5	199 F g^{-1} at 1 A g^{-1}	42.83 at the P of 0.43	8.5 at the E of 12.99	80.4% after10000 cycles at 5 A g^{-1}	14
(Ni,Co)Se_2/NiCo-LDH//PC	1.65	102 F g^{-1} at 2 A g^{-1}	35 at the P of 1.65	8.25 at the E of 24	90% after 5000 cycles at 5 A g^{-1}	15
CCCH@ NiCo-LDH NWAs@Au–CuO/Cu//VN/CFs	1.7	92.5 F g^{-1} at 2 mA	35.0 at the P of 1.41	13.9 at the E of 27.4	94.8% after 10000 cycles	16
A-Co$(OH)_2$@NiCo-LDH//AC	1.7	100.38 F g^{-1} at 2 A g^{-1}	40.61 at the P of 1.78	23.55 at the E of 28.59	81.23% after 10000 cycles at 5 A g^{-1}	**This work**

Table S3. The electrochemical performance comparison of the state-of-the-art alkaline Zn-ion batteries based on transition-metal compounds

AZIBs	Voltage window (V)	Specific capacity (mAh g^{-1})	Energy density (*E*, Wh kg^{-1})	Power density (*P*, kW kg^{-1})	Capacitance retention rate	Ref.
Co_3O_4/Ni//Zn/CC	1.78	162 mAh g^{-1} at 1 A g^{-1}	235	-	80 % after 2000 cycles at 1 A g^{-1}	[17]
N-rGO)/Fe_2O_3	1.45	249 mAh g^{-1} at 1 A g^{-1}	50.2 at the *P* of 0.485	16.1 at the *E* of 9.7	91.5 % after 5000 cycles at 3 A g^{-1}	[18]
NiO/CF//ZnO/CF	1.9	203 mAh g^{-1} at 0.26 A g^{-1}	355.7 at the *P* of 17.9	-	72.9 % after 2400 cycles at 5 mA cm^{-1}	[19]
NiAlCo LDH/CNT//Zn	1.75	354 mAh g^{-1} at 6.7A g^{-1}	274 at the *P* of 16	-	94 % after 2000 cycles at 66.7 A g^{-1}	[20]
A-$Co(OH)_2$@NiCo-LDH//Zn	1.85	309.3 mAh g^{-1} at 0.2 A g^{-1}	489.6 at the *P* of 0.38	9.64 at the *E* of 321.2	76.68 % after 1000 cycles at 5 A g^{-1}	**This work**

References

1 S. Liu, Y. Yin, D. Ni, K. S. Hui, M. Ma, S. Park, K. N. Hui, C.-Y. Ouyang and S. C. Jun, New insight into the effect of fluorine doping and oxygen vacancies on electrochemical performance of co_2mno_4 for flexible quasi-solid-state asymmetric supercapacitors, *Energy Storage Mater.*, 2019, **22**, 384-396.

2 H. Wang, S. Zhang and C. Deng, In situ encapsulating metal oxides into core-shell hierarchical hybrid fibers for flexible zinc-ion batteries toward high durability and ultrafast capability for wearable applications, *ACS Appl. Mater. Interfaces*, 2019, **11**, 35796-35808.

3 H. B. Aiyappa, J. Masa, C. Andronescu, M. Muhler, R. A. Fischer and W. Schuhmann, Mofs for electrocatalysis: From serendipity to design strategies, *Small Methods*, 2019, **3**, 1800415.

4 W. Guo, C. Yu, S. Li, X. Song, H. Huang, X. Han, Z. Wang, Z. Liu, J. Yu, X. Tan and J. Qiu, A universal converse voltage process for triggering transition metal hybrids in situ phase restruction toward ultrahigh-rate supercapacitors, *Adv. Mater.*, 2019, **31**, 1901241.

5 S. F. Li, C. Yu, Y. Yang, X. D. Song, S. M. Chen, L. Song, B. Qiu, J. Yang, H. W. Huang, W. Guo, C. T. Zhao, M. D. Zhang and J. S. Qiu, Phosphate species up to 70% mass ratio for enhanced pseudocapacitive properties, *Small*, 2018, **14**.

6 V. Augustyn, P. Simon and B. Dunn, Pseudocapacitive oxide materials for high-rate electrochemical energy storage, *Energy Environ. Sci.*, 2014, **7**, 1597.

7 B. Ramulu, S. C. Sekhar, G. Nagaraju, S. J. Arbaz and J. S. Yu, Unveiling one-dimensional mixed-metallic oxysulfide nanorods as an advanced cathode material for hybrid supercapacitors, *J. Power Sources*, 2021, **482**, 228944.

8 L. Q. Mai, A. Minhas-Khan, X. Tian, K. M. Hercule, Y. L. Zhao, X. Lin and X. Xu, Synergistic interaction between redox-active electrolyte and binder-free functionalized carbon for ultrahigh supercapacitor performance, *Nat. Commun.*, 2013, **4**, 2923.

9 X. Feng, Y. Huang, C. Li, X. Chen, S. Zhou, X. Gao and C. Chen, Controllable synthesis of porous $NiCo_2O_4$/NiO/Co_3O_4 nanoflowers for asymmetric all-solid-state supercapacitors, *Chem. Eng. J.*, 2019, **368**, 51-60.

10 S. K. Hussain, G. Nagaraju, S. C. Sekhar and J. S. Yu, Selective combination of highly porous hollow structured battery-type bimetallic spinel oxides with improved redox chemistry for electrochemical hybrid capacitor, *Energy Storage Mater.*, 2020, **27**, 405-417.

11 W. Guo, C. Yu, S. Li, X. Song, Y. Yang, B. Qiu, C. Zhao, H. Huang, J. Yang, X. Han, D. Li and J. Qiu, A phase transformation-resistant electrode enabled by a MnO_2-confined effect for enhanced energy storage, *Adv. Funct. Mater.*, 2019, **29**, 1901342.

12 Y. Tang, H. Shen, J. Cheng, Z. Liang, C. Qu, H. Tabassum and R. Zou, Fabrication of oxygen-vacancy abundant nimn-layered double hydroxides for ultrahigh capacity supercapacitors, *Adv. Funct. Mater.*, 2020, **30**, 1908223.

13 X. Gao, X. Liu, D. Wu, B. Qian, Z. Kou, Z. Pan, Y. Pang, L. Miao and J. Wang, Significant role of al in ternary layered double hydroxides for enhancing electrochemical performance of flexible asymmetric supercapacitor, *Adv. Funct. Mater.*, 2019, **29**, 1903879.

14 B. Li, P. Gu, Y. Feng, G. Zhang, K. Huang, H. Xue and H. Pang, Ultrathin nickel-cobalt phosphate 2D nanosheets for electrochemical energy storage under aqueous/solid-state electrolyte, *Adv. Funct. Mater.*, 2017, **27**, 1605784.

15 X. Li, H. Wu, A. M. Elshahawy, L. Wang, S. J. Pennycook, C. Guan and J. Wang, Cactus-like nicop/NiCo-OH 3D architecture with tunable composition for high-performance electrochemical capacitors, *Adv. Funct. Mater.*, 2018, **28**, 1800036.

16 Y. Guo, X. Hong, Y. Wang, Q. Li, J. Meng, R. Dai, X. Liu, L. He and L. Mai,

Multicomponent hierarchical cu-doped NiCo-LDH/CuO double arrays for ultralong-life hybrid fiber supercapacitor, *Adv. Funct. Mater.*, 2019, **29**, 1809004.

17 X. W. Wang, F. X. Wang, L. Y. Wang, M. X. Li, Y. F. Wang, B. W. Chen, Y. S. Zhu, L. J. Fu, L. S. Zha, L. X. Zhang, Y. P. Wu and W. Huang, An aqueous rechargeable Zn//Co_3O_4 battery with high energy density and good cycling behavior, *Adv. Mater.*, 2016, **28**, 4904-4911.

18 Y. Zhu, J. Li, X. Yun, G. Zhao, P. Ge, G. Zou, Y. Liu, H. Hou and X. Ji, Graphitic carbon quantum dots modified nickel cobalt sulfide as cathode materials for alkaline aqueous batteries, *Nano-Micro Lett.*, 2020, **12**, 1-18.

19 J. Liu, C. Guan, C. Zhou, Z. Fan, Q. Ke, G. Zhang, C. Liu and J. Wang, A flexible quasi-solid-state nickel-zinc battery with high energy and power densities based on 3D electrode design, *Adv. Mater.*, 2016, **28**, 8732-8739.

20 M. Gong, Y. Li, H. Zhang, B. Zhang, W. Zhou, J. Feng, H. Wang, Y. Liang, Z. Fan, J. Liu and H. Dai, Ultrafast high-capacity nizn battery with nialco-layered double hydroxide, *Energy Environ. Sci.*, 2014, **7**, 2025.